AIAA JOURNAL
Vol. 30, No. 4, April 1992

Influence of Geometric Nonlinearities on Skin-Stiffener Interface Stresses

D. Cohen*
Hercules Aerospace Company, Inc., Magna, Utah 84044
and
M. W. Hyer†
Virginia Polytechnic Institute and State University, Blacksburg, Virginia 24061

A method for computing skin-stiffener interface stresses in stiffened composite panels is developed. Both geometrically linear and nonlinear analyses are considered. Particular attention is given to the flange termination region where stresses are expected to exhibit unbounded characteristics. The method is based on a finite element analysis and an elasticity solution. The finite element analysis is standard, whereas the elasticity solution is based on an eigenvalue expansion of the stress functions. The eigenvalue expansion is assumed to be valid in the local flange termination region and is coupled with the finite element analysis using collocation of stresses on the local region boundaries. The results indicate that the inclusion of geometric nonlinearities is very important for an accurate determination of the interface stresses. Membrane flattening of the panel tends to reduce the tendency of the stiffener to separate.

Introduction

THE use of composite materials in primary structures poses new challenges to both the stress analyst and the designer. In skin-stiffener combinations that have been cocured or secondarily bonded together, it has been observed that failure is often initiated by skin-stiffener separation.[1] To predict and design against this type of failure, it is important to be able to assess stresses at the skin-stiffener interface. A particularly troublesome region of the interface is the region where the stiffener flange terminates. As with the free edge of a composite laminate, the stresses at the flange termination region can become unbounded. In previous papers,[2,3] the application of an elasticity solution to the calculation of skin-stiffener interface stresses in the geometrically linear range of structural deflections was discussed. More specifically, a method was outlined by which a generalized plane deformation elasticity solution could be used in combination with standard finite element calculations to predict stresses in the interface region. The elasticity solution was valid in the localized region near the flange termination point, whereas the finite element calculations were valid for the remainder of the interface. The elasticity solution used an eigenvalue expansion of the stress functions to calculate the stresses. Though useful for contributing to the understanding of some aspects of skin-stiffener interaction, the geometrically linear analysis was limited. Generally, the deformations of stiffened composite skins are large enough that geometric nonlinearities need to be considered in any realistic analysis. Hence, in the present paper, the methodology developed in the previous papers[2,3] is extended to include the effects of geometric nonlinearities on the calculation of skin-stiffener interface stresses. In this extension to the previous work, it is assumed that the strains are small, the material behavior is linear elastic, and the rotations are finite but moderate. One of the highlights of the present work is a comparison of the linear and nonlinear analyses and the misconceptions incurred by using only linear analyses. The inclusion of geometric nonlinearities represents a contribution to the study of problems of this type.

Problem Definition and Analysis Procedure

The particular problem studied is a pressure-loaded stiffener-skin plate configuration that is clamped on all four sides. Figure 1 shows the configuration. The pressure loading on the plate is actually a vacuum loading on the lower surface as used in an earlier study.[4] Though the results for that study will not be discussed here, that study was the motivation for the present study. In the analysis to be presented, special attention is given to the analysis of the skin-stiffener cross section.

As can be seen in Fig. 1, the stiffener is of the inverted T type, consisting of a flange, which is attached to the skin, and a web. It is assumed that the bond between the flange and the skin is perfect and the bond line is of zero thickness. Though stiffened skins are often subjected to both applied transverse pressure and applied in-plane loads, only an applied pressure load is considered here. The methodology can most certainly be extended to more general loadings.

The analysis procedure to be discussed consists of three steps. These steps are the following: a structural level analysis, a substructural level analysis, and a local level analysis. These three steps are depicted in Figs. 2a–2c, respectively.

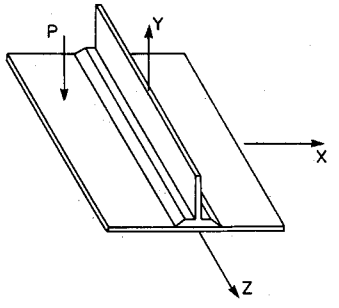

Fig. 1 Skin-stiffener plate configuration.

Presented as Paper 88-2217 at the 29th AIAA/ASME/ASCE/AHS Structures, Structural Dynamics, and Materials Conference, Williamsburg, VA, April 18–20, 1988; received Aug. 10, 1988; revision received March 11, 1991; accepted for publication April 18, 1991.

*Staff Engineer, Bacchus Works. Member AIAA.
†Professor, Department of Engineering Science and Mechanics. Associate Fellow AIAA.

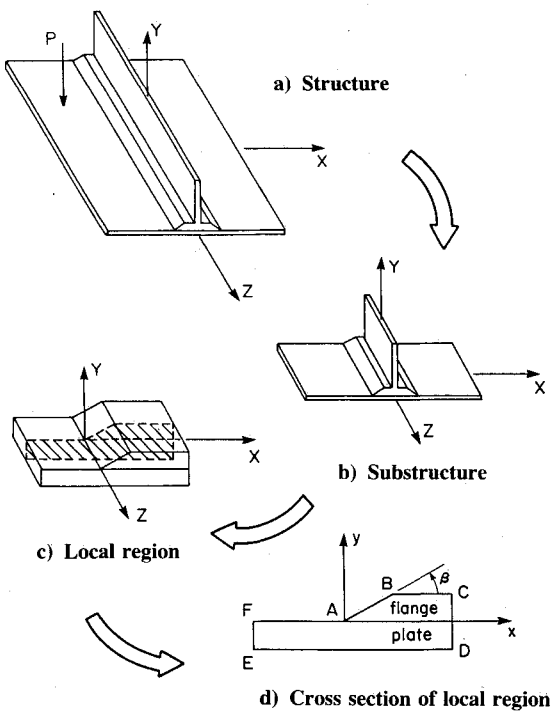

Fig. 2 Structure-substructure-local analysis procedure.

The structural level analysis consists of a two-dimensional structural level finite element analysis of the entire stiffened plate. The substructural analysis is a more detailed three-dimensional finite element analysis of a typical cross section in the central region of the stiffened plate. The local analysis is a rigorous elasticity solution of the flange termination region, a region suspected of having high stresses and high stress gradients. The three levels of analysis are coupled together as follows. The two-dimensional structural level analysis is conducted using whatever applied loading and boundary conditions are of interest (here, a pressure loading and clamped boundaries). Displacements on what are the boundaries of the three-dimensional substructural region are computed from the structural level analysis. These displacements are then used as boundary conditions for the three-dimensional substructural analysis. These displacement boundary conditions, produced by the applied loading and boundary conditions of the structural level analysis, are what tie the structural level and substructural level analyses together. In turn, the stresses from the three-dimensional substructural analysis on what are the boundaries of the local region are used in a stress-based boundary collocation scheme to produce the elasticity solution. The stresses on the collocation boundary are what couple the substructural and local levels of analysis. Fortunately, the majority of skin-stiffener interface separations have been observed to occur toward the central regions of panels, a region where the analysis is indeed valid.

Both the structural and the substructural analyses are conducted using a standard finite element code, in particular, the commercially available engineering analysis language (EAL) code.[5] The local elasticity analysis is based on an eigenvalue expansion of the stress functions and follows the work of Lekhnitskii,[6] Wang and Choi,[7] and Delale.[8] The assumption that leads to a tractable elasticity solution is the assumption that in the localized region the stresses do not vary with the longitudinal coordinate z, i.e., the coordinate in the stiffener direction (see Figs. 1 and 2). Thus, the analysis must be confined to regions away from the ends of the plate, regions where the variations of the stresses with the longitudinal coordinate are not particularly strong. This independence of the stresses and, hence, the strains on the longitudinal coordinate categorizes the problem as one of generalized plane deformation. The analysis of the local region accurately accounts for differences in material properties between the skin and flange, variations in the flange termination angle β (Fig. 2d), and differences in skin and flange thicknesses. Thus, the local analysis involves all of the parameters felt to influence skin-stiffener interface stresses. With the generalized plane deformation assumption, the analysis of the localized region can be represented by an analysis of the cross-hatched plane in Fig. 2c. In Fig. 2d, this plane is expanded and the plane is shown to be bounded by points A, B, C, D, E, and F.

In the sections that follow, each step of the three-step analysis procedure is discussed in greater detail. The next section briefly reviews the geometrically linear local elasticity analysis. This sets the stage for the discussion of the extension of the local elasticity solution to include geometric nonlinearities. Next, more detail regarding the structural and substructural analyses is presented. Finally, results are presented that demonstrate the significance of including geometric nonlinearities in the calculation of skin-stiffener interface stresses.

Geometrically Linear Local Elasticity Analysis

The local region is considered to be dominated by the facts that the flange terminates at a known angle β relative to the skin, the flange and the skin are generally made of different materials, and they are perfectly bonded together with a bond line of zero thickness. The material properties of the skin and the flange are each assumed to be orthotropic. Though the flange and the skin are made of multiple layers of fiber-reinforced material, in each case the effects of the multiple layers are smeared to obtain equivalent orthotropic material properties. These properties are assumed to be valid through the thickness of the flange and the skin. Essentially, the smearing technique assumes that the details of the interaction between the skin and the flange are governed more by the overall material properties of these two subcomponents rather than by the material properties of the top layer of the skin that is adjacent to the bottom layer of the flange. It should be noted that despite smearing, the differences in elastic properties due to differences in stacking sequences, e.g., differences in D_{22}, can still be accounted for in the theory. In this study, the flange termination region is cast in such a way that the flange termination region is a special case of bimaterial wedge. As in previous studies,[7-10] the wedge is analyzed as if it were a semi-infinite domain. This can be visualized by allowing points B, C, D, E, and F in Fig. 2d to move to infinity in the various directions. The results of the analysis of the semi-infinite bimaterial domain are then actually applied over the finite region bounded by ABCDEF of Fig. 2d. The stress boundary conditions on AB and FA are satisfied exactly, whereas the stress boundary conditions on the remainder of the contour are made to match, in the least-squares sense, the contour conditions as calculated by the substructural analysis.

The solution to the semi-infinite bimaterial domain just described is given in Refs. 2 and 3 for the geometrically linear analysis. The solution is derived in the form of eigenvalue expansion of two stress functions $F(x, y)$ and $\psi(x, y)$ as follows:

$$F(x, y) = C \frac{(x + \mu y)^{\lambda+2}}{(\lambda + 1)(\lambda + 2)} \tag{1a}$$

$$\psi(x, y) = D \frac{(x + \nu y)^{\delta+1}}{(\delta + 1)} \tag{1b}$$

where μ and ν are two known material parameters and C, D, λ, and δ are unknown complex constants that must be determined. The stress equilibrium equations are satisfied identically if the stresses are written in terms of the stress functions as

$$\sigma_x = \frac{\partial^2 F}{\partial y^2} \tag{2a}$$

$$\sigma_y = \frac{\partial^2 F}{\partial x^2} \tag{2b}$$

$$\tau_{xy} = -\frac{\partial^2 F}{\partial x \partial y} \tag{2c}$$

$$\tau_{yz} = -\frac{\partial \psi}{\partial x} \tag{2d}$$

$$\tau_{xz} = -\frac{\partial \psi}{\partial y} \tag{2e}$$

The equations that govern $F(x, y)$ and $\psi(x, y)$ are derived by utilizing the constitutive equations and integrating the strain-displacement relations. For orthotropic materials, the equations that govern $F(x, y)$ and $\psi(x, y)$ are

$$\beta_{22}\frac{\partial^4 F}{\partial x^4} + (2\beta_{12} + \beta_{66})\frac{\partial^4 F}{\partial x^2 \partial y^2} + \beta_{11}\frac{\partial^4 F}{\partial y^4} = 0 \tag{3a}$$

$$\beta_{44}\frac{\partial^2 \psi}{\partial x^2} + \beta_{55}\frac{\partial^2 \psi}{\partial y^2} = -2B_4 \tag{3b}$$

where β_{ij} are reduced compliances and B_4 is a constant of integration. The decoupling of the two equations governing the stress functions is a distinct characteristic of orthotropic materials. The equation governing $F(x, y)$ is homogeneous, and the equations for $\psi(x, y)$ involve a particular solution. Upon substitution of Eqs. (1a) and (1b) into Eqs. (3a) and (3b), respectively, a general form of the solution of the two stress functions that govern the semi-infinite domain is obtained. This form can be written as,

$$F(x, y) = F^{(e)}(x, y) + F^{(a)}(x, y) \tag{4a}$$

$$\psi(x, y) = \psi^{(e)}(x, y) + \psi^{(a)}(x, y) + \psi^{(p)}(x, y) \tag{4b}$$

where the superscripts (e), (a), and (p) represent the eigenvalue expansion, the auxiliary, and the particular solutions, respectively. The solutions are given by

$$F^{(e)}(x, y) = \sum_{k=1}^{4} C_k \frac{(x + \mu_k y)^{\lambda+2}}{(\lambda + 1)(\lambda + 2)} \tag{5a}$$

$$F^{(a)}(x, y) = b_1 x^3 + b_2 x^2 y + b_3 x y^2 + b_4 y^3 + b_5 x^2 + b_6 x y + b_7 y^2 \tag{5b}$$

$$\psi^{(e)}(x, y) = \sum_{k=1}^{2} D_k \frac{(x + \nu_k y)^{\delta+1}}{\delta + 1} \tag{5c}$$

$$\psi^{(a)}(x, y) = b_8 x + b_9 y \tag{5d}$$

$$\psi^{(p)}(x, y) = b_{10} x^2 + b_{11} y^2 \tag{5e}$$

The four μ_k and two ν_k are determined from the two equations

$$\beta_{22} + (2\beta_{12} + \beta_{66})\mu^2 + \beta_{11}\mu^4 = 0 \tag{6a}$$

$$\beta_{55}\nu^2 + \beta_{44} = 0 \tag{6b}$$

There is a solution of the form given by Eqs. (5) and (6) for the localized region of the flange, and another solution of the same form for the localized region of the skin. In the above, the b_i, $i = 1,11$ are unknown real constants and λ, δ, C, and D constitute two sets of eigenvalues and associated eigenvectors. That these latter quantities are eigenvalues and eigenvectors is not known until the stresses and displacements are written in terms of the general forms of the solution, and the boundary and interface conditions are applied to the local flange-skin interface region. These boundary and interface conditions are applied to the semi-infinite domain associated with Fig. 2d. The conditions applied to the flange-skin interface region are the following: 1) traction free conditions along boundaries AB and FA, and 2) traction and displacement continuity across the skin-flange interface. Imposition of these conditions leads to a homogeneous set of equations that can be satisfied by an infinite number of λ and δ. For each value of λ, the four C_k are determined to within an unknown constant. Likewise, for each value of δ, the two D_k are determined to within an unknown constant. It can be shown that the eigenvalue expansion portions of the solution can be written as double series of the form[11]:

$$F_i^{(e)}(x, y) = \sum_{n=1}^{\infty} \left\{ c_n \operatorname{Re}\left[\sum_{k=1}^{4} c_{nk}^{(i)} \frac{(x + \mu_k^{(i)} y)^{\lambda_n + 2}}{(\lambda_n + 1)(\lambda_n + 2)} \right] + c_n' \operatorname{Im}\left[\sum_{k=1}^{4} c_{nk}^{(i)} \frac{(x + \mu_k^{(i)} y)^{\lambda_n + 2}}{(\lambda_n + 1)(\lambda_n + 2)} \right] \right\} \tag{7a}$$

$$\psi_i^{(e)}(x, y) = \sum_{n=1}^{\infty} \left\{ d_n \operatorname{Re}\left[\sum_{k=1}^{2} d_{nk}^{(i)} \frac{(x + \nu_k^{(i)} y)^{\delta_n + 2}}{(\delta_n + 1)} \right] + d_n' \operatorname{Im}\left[\sum_{k=1}^{2} d_{nk}^{(i)} \frac{(x + \nu_k^{(i)} y)^{\delta_n + 1}}{(\delta_n + 1)} \right] \right\} \tag{7b}$$

where $i = 1, 2$ corresponds to materials 1 and 2, the flange and skin, respectively. In addition, c_n, c_n', d_n, and d_n' are unknown real coefficients, whereas $c_{nk}^{(i)}$ $i = 1, 2$; $k = 1, 4$ and $d_{nk}^{(i)}$ $i = 1, 2$; $k = 1, 2$ are known magnitudes of the components of the nth eigenvector associated with materials 1 and 2, respectively.

At this point, some important issues need to be emphasized. The decoupling of the two stress functions leads to two independent problems: one involving u, v, σ_x, σ_y, and τ_{xy}; and the other involving w, τ_{xz}, and τ_{yz}. The displacements u, v, and w are the displacements in the x, y, and z directions, respectively. The former problem is referred to as the in-plane problem, whereas the latter problem is referred to as the out-of-plane problem. The in-plane problem involves the eigenvalues λ_n and associated eigenvectors $c_{nk}^{(i)}$, whereas the out-of-plane problem involves the eigenvalues δ_n and the associated eigenvectors $d_{nk}^{(i)}$. The λ_n are, in general, complex, whereas the δ_n are real. Considering the functional form of $F(x, y)$ and $\psi(x, y)$ and the fact that both the stresses and displacements are derived from the derivatives of these functions, it is possible that for certain values of λ_n and δ_n both the stresses and displacements will exhibit unbounded characteristics near the termination of the flange-skin interface, point A in Fig 2d. This is physically impossible. To have bounded displacements, the real part of the eigenvalues must be > -1. Even with this restriction, the stresses may be unbounded. This leads to severe stress gradients near point A. For the class of problems considered here, it appears that only the λ lead to unbounded stresses. The stresses associated with δ are bounded. In addition, it can be shown that, with no twisting of the plate about the z axis, with orthotropic materials there are no out-of-plane stresses τ_{xz} and τ_{yz}. Therefore, for the remainder of this discussion, only the in-plane problem will be considered.

Continuing with the discussion of the problem solution for the pressurized plate, the application of the boundary and interface conditions also provides information on some of the b_i of Eqs. (5), many of the b_i being zero. The determination of the remaining b_i and the determination of the unknown magnitudes of the eigenvectors, i.e., determining the c_n, c_n', d_n, and d_n', depends on interfacing the local solution with the substructural solution. Here, it is assumed that the eigenvalue expansion, which is developed for the semi-infinite domain, is valid in the finite region defined by ABCDEF in Fig. 2d. In addition, the expansion is represented by a finite number

of terms N in the series. With these assumptions, the response in the local region can be determined by using information from the substructural analysis. In particular, the local analysis relies on specifying the axial extension e^o and curvature κ^o in the z direction for the local region. (This is a result of the generalized plane deformation assumption.) This kinematic information is obtained by reducing displacement data from the substructural model. With this information, two of the b_i are found. They are

$$b_4^{(2)} = \frac{K\kappa^o}{3a_{33}^{(2)}} \tag{8a}$$

$$b_7^{(2)} = K\left[\frac{e^o}{a_{33}^{(2)}}\right] \tag{8b}$$

where

$$K = \frac{1}{2}\left[\frac{a_{13}^{(1)}a_{33}^{(2)} - a_{13}^{(2)}a_{33}^{(1)}}{\beta_{11}^{(2)}a_{33}^{(1)}}\right] \tag{8c}$$

The $a_{ij}^{(k)}$ are components of the compliance matrix. The remaining unknown b_i and the unknown c_n and c_n', $n = 1, N$, are determined by matching on contour BCDEF the stresses written in terms of these unknowns with the same stresses as computed by the substructural analysis. This procedure is discussed in greater detail in the following sections and in Ref. 11.

Geometrically Nonlinear Local Elasticity Analysis

For a thin flexible structure, such as the stiffened composite panels considered here, it is valid to assume that the strains are much smaller than unity and that the rotations are also smaller than unity, but larger than the strains. This leads to neglecting the strains and rotations compared to unity and the strains compared to the rotations. For the problem here, only rotations about the z axis are retained. Thus, an element within the cross section in the deformed state may be represented by its original undeformed shape but in a rotated and translated position. The normal and shear stresses generated by the deformation are perpendicular and parallel, respectively, to the boundaries of the element and are, thus, also rotated and translated. Furthermore, a local orthogonal x-y-z coordinate system attached to an element transforms into an orthogonal $\bar{x}$-$\bar{y}$-$\bar{z}$ coordinate system by rotation. Because of these considerations, the local elasticity solution outlined in the previous section can be formulated in the rotated coordinate system $\bar{x}$-$\bar{y}$-$\bar{z}$ and the governing equations of elasticity will appear exactly as the governing equations for the linear case. The localized skin-stiffener region in its original shape but undergoing rigid-body rotations is shown in exaggerated form in Figs. 3. Here, it is assumed that the rotations in the local region are independent of location within the region. If the rotations were not independent of location within the region, Fig. 3b could not be drawn and the extension of the linear analysis would not be valid. Since Fig. 3b is assumed to represent the problem being considered, the procedure outlined previously for determination of the coefficients c_n and c_n' in the eigenfunction expansion, Eq. (7a), is then valid for the geometrically nonlinear problem, provided it is performed in the deformed body state. This is the primary difference between the linear and nonlinear analyses.

Structure-Substructure-Local Analysis Procedure

In the structural analysis, the stiffened composite plate is discretized using 4-node plate elements. Each element of this type has five degrees of freedom, namely, u, v, w, $\partial v/\partial z$, and $\partial v/\partial x$. As mentioned previously, the skin, the flange region, and the stiffener web are modeled with orthotropic material behavior. The flange stiffness is lumped into the plate stiffness

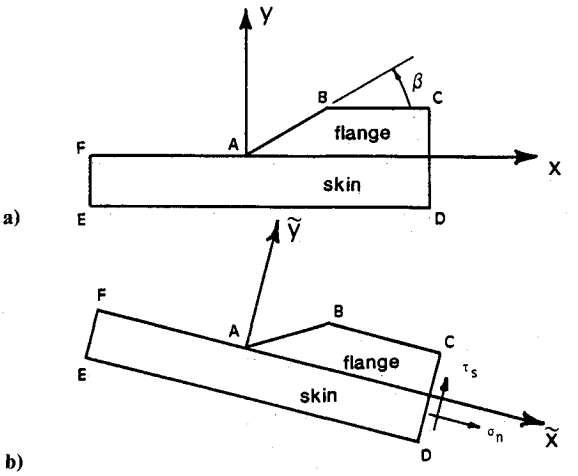

Fig. 3 Finite rotation of local region: a) undeformed; b) deformed.

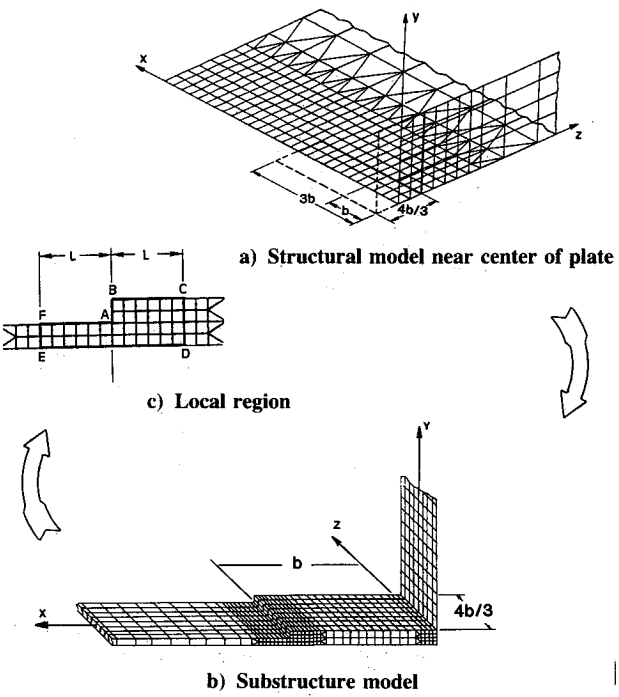

Fig. 4 Structure to substructure analysis procedure and finite element discretization.

in the stiffener area, and the web is considered to be a plate connected along its edge to the skin. The skin, the skin-flange region, and the web are assumed to respond in accordance with classical laminated plate theory. The material data are specified in the form of laminate stiffness matrices, A, B, and D. In the structural level analysis, all of the extension and bending-twisting coupling terms are set to zero. These terms include B_{16}, B_{26}, D_{16}, and D_{26}. For symmetric laminates, such as the one considered here, $B_{16} = B_{26} = 0$ for both the skin and the stiffener. On the other hand, neither D_{16} nor D_{26} are zero. However, they tend to be small relative to D_{11}, D_{12}, D_{22}, and D_{66}. Given these material restrictions, and the geometry and loading conditions considered, it is only necessary to analyze one-quarter of the plate using the two planes of symmetry, i.e., the planes $[x, y, 0]$ and $[0, y, z]$.

To provide accurate boundary conditions for the substructure analysis, the generally coarse structural level mesh was refined at the central region of the plate. Figure 4a illustrates such a coarse mesh refinement in the plate's central region. Since the displacements from the structural level analysis are used as boundary conditions for the three-dimensional sub-

Table 1 Displacement boundary conditions imposed in the substructure model

Boundary	Specified displacements
$(x, y, -2b/3)$	u, v, and w
$(x, y, +2b/3)$	u, v, and w
$(3b, y, z)$	u, v, and w
$(0, y, z)$	$u = 0$

structural analysis, convergence of these displacements was studied. A convergence study of nodal displacements indicated that a coarse mesh that was refined twice in the region led to the convergence of these nodal quantities in this region.

The substructural analysis is conducted at the plate center location. The region for which the substructural analysis is performed is indicated by the area outlined by the heavy line in Fig. 4a. Figure 4b shows a schematic discretization of the substructure finite element model. The model extends a distance $2b/3$ both sides of the symmetry plane $[x, y, 0]$ and thus has a total width of $4b/3$ (where b is the flange half-width). The model is discretized with eight solid elements in the z direction and includes details of any flange tapering. The displacement boundary conditions imposed on the substructure model are described in Table 1. The values for u, v, and w are determined from the structural analysis displacement data by applying the Kirchhoff assumption. That is,

$$u(x, y, z) = u^o(x, z) - \frac{\partial v^o}{\partial x} y \tag{9a}$$

$$v(x, y, z) = v^o(x, z) \tag{9b}$$

$$w(x, y, z) = w^o(x, z) + \frac{\partial v^o}{\partial z} y \tag{9c}$$

where u^o, v^o, and w^o are the displacements of the skin midsurface as determined from the structural level analysis.

Finally, a unique local elasticity solution for a given pressure and boundary conditions is obtained by evaluating the unknown coefficients c_n and c_n' using a boundary collocation technique. In the collocation procedure, the normal σ_n and tangential τ_s stresses shown in Figs. 3 are collocated along the closed contour ABCDEFA shown in Fig. 4c. In reality, collocation takes place only along boundaries BC, CD, DE, and EF. The conditions of stress-free boundaries along AB and FA are satisfied exactly by the elasticity solution. Boundary BC is taken as a stress-free face, whereas boundary DE is subjected to uniform normal traction representing the applied vacuum. The stresses along the internal boundaries CD and EF are those determined by the substructure finite element analysis. It should be pointed out that in the nonlinear analysis σ_n and τ_s are the normal and tangential stresses for the rotated local region boundaries. In the procedure, the collocation points are uniformly spaced along the contour. The boundaries CD and EF are placed at distance L from point A. This distance, shown in Fig. 4c, was chosen according to the condition that σ_y and τ_{xy}, as computed by the substructure finite element analysis, must be continuous across the skin-flange interface. That is, the stresses σ_y and τ_{xy} computed by the elements on either side of the interface in the skin and flange must yield the same value to within 5%. The theory of elasticity stipulates that these two components of stress are exactly continuous across the interface. This 5% condition assures that the skin-stiffener interlaminar stresses computed by the substructure finite element analysis satisfy this condition to within a small tolerance and, thus, are accurate in the skin-stiffener interface region outside of the local region. Based on this 5% condition, it was determined that for the mesh used in the present investigation L should be about 1.5 times the combined thickness of the skin and the flange. In the boundary collocation procedure, the normal and shear stresses along the contour BCDEF are written in terms of the unknown coefficients c_n and c_n' in a truncated eigenfunction expansion. These stresses are matched with the same stress components calculated by the substructure finite element analysis. For the specific problem here, the collocation at M points around the boundary BCDEF leads to $2M$ simultaneous equations from which the $2N$ unknown coefficients are determined. The use of more collocation points, i.e., $M > N$, leads to an overdetermined set of equations. Solution of these equations produces the $2N$ unknown coefficients c_n and c_n', which satisfy all boundary conditions on contour BCDEF in a least-squares sense.

Results

Using the methodology outlined earlier for computing skin-stiffener interface stresses, the importance of geometric nonlinearities can be evaluated. The results that are presented in the following sections are for a plate clamped on all four edges with a single inverted T stiffener, as depicted by Fig. 1. The plate is subjected to three levels of transverse pressure, 6.9, 69, and 138 kPa (1, 10, and 20 psi), respectively. The 69-kPa pressure level nominally represents the operating aircraft fuselage pressure, whereas the 138-kPa pressure represents the design level. The 6.9-kPa pressure level is used since the linear and nonlinear analyses should produce similar results at this pressure level, and linear results for other pressure levels can be scaled from the 6.9-kPa analysis. To study the influence of geometric nonlinearities on the interface stresses, the following skin-stiffener configuration is considered: 1) a stiffener web height of 38 mm (1.5 in.), 2) a flange width $2b$ = 38 mm (1.5 in.), 3) a flange thickness t_f = 1 mm (0.040 in.), and 4) a skin thickness t_s = 1 mm (0.040 in.). For this configuration, the stiffener is constructed of a quasi-isotropic laminate with $(\pm 45/0/90)_s$ layup sequence. The skin is orthotropic with a laminate layup of $(\pm 45/90_2)_s$. The flange termination angle β is 90 deg. Fiber angle is with respect to the $+z$ axis.

Figures 5 illustrate the skin-stiffener interface stresses σ_y and τ_{xy} along the entire flange-skin interface length, as well as details along the flange termination region. As can be seen, the severe stresses and stress gradients occur near the flange termination region for both the peel σ_y and shear τ_{xy} stresses. In Figs. 5, stresses are normalized by the applied pressure p. The distance x from the flange terminus (point A of Fig. 2d) is normalized either by b, the flange half-width, or by t_s, the skin thickness.

The most significant point to emerge from Figs. 5a–5d is the dependence of the distribution and magnitude of stresses on the applied pressure level when geometric nonlinearities are considered. By definition, for a linear analysis, the normalized interface stress variation throughout the flange termination region is independent of the applied pressure. The results for 6.9, 69, and 138 kPa are coincident. However, with geometric nonlinearities included, differences in the characteristics of the stress distributions are observed for different pressure levels. Focusing on the peel stress, Fig. 5b, the linear and 6.9-kPa nonlinear analysis produces stresses of similar magnitude, and the distributions are similar. However, the nonlinear analysis for 69 kPa and the linear analysis show significantly different results. The 138-kPa nonlinear analysis deviates even more from the linear analysis. With increasing pressure, geometrically nonlinear effects tend to reduce the magnitude of the stress reversal and drive the steep gradient more toward the flange terminate point. For the shear stress, Fig. 5d, geometrically nonlinear effects also drive the sharp stress gradient toward the flange termination point. In all cases and for both stress components, the large stress gradients appear to be confined primarily to the local flange termination region. Under the web, there is a local maximum in the peeling stress and the maximum value tends to decrease slightly with increases in pressure. The shear stress is zero directly under the web. Relations like the one shown in Figs.

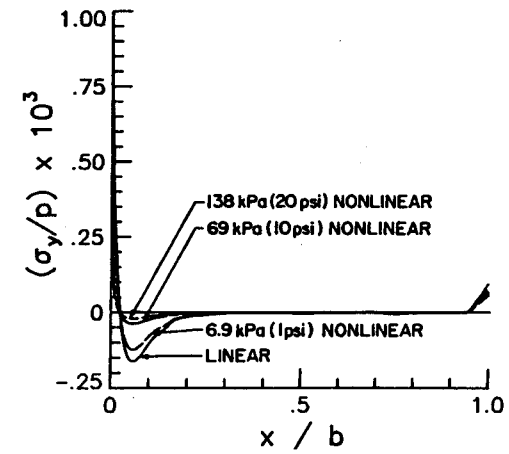

a) Peeling stress along entire flange length

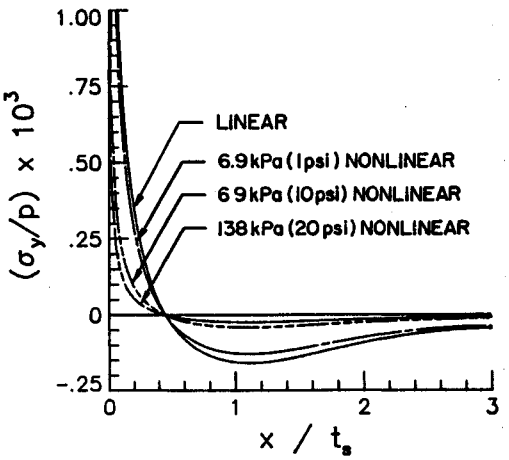

b) Peeling stress in flange termination region

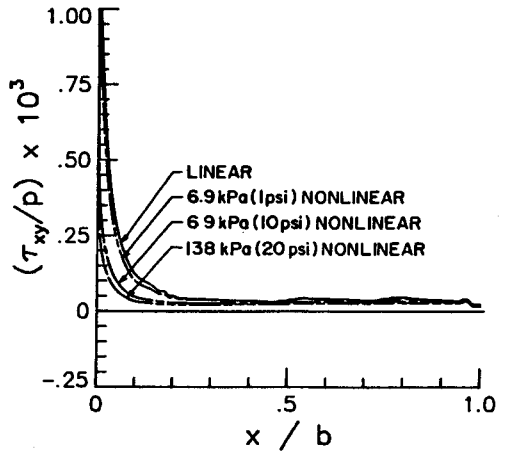

c) Shearing stress along entire flange length

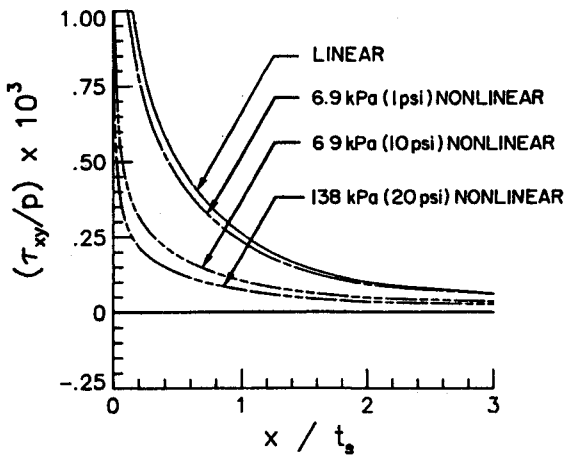

d) Shearing stress in flange termination region

Fig. 5 Variation of skin-stiffener interface stresses, geometrically linear and nonlinear analyses.

5a and 5c indicate that the load transfer from the skin to the stiffener is confined to either a very short portion of the flange width or directly under the web.

To facilitate a better demonstration of this important nonlinear interaction between skin-stiffener interface stresses and applied pressure, stress eigenfactors (SEF) are used. These SEF are defined as[7]

$$K_y = \lim_{x \to 0} x^{\lambda_1} \sigma_y(x, 0; \lambda_1) \tag{10a}$$

$$K_{xy} = \lim_{x \to 0} x^{\lambda_1} \tau_{xy}(x, 0; \lambda_1) \tag{10b}$$

where K_y and K_{xy} are the peeling and shearing stress eigenfactors, respectively, and λ_1 is the first eigenvalue used in the stress function expansion. The stress eigenfactor is a measure of how rapidly the stresses become unbounded as the flange termination point is approached. The factor can be used as a measure of the severity of the interaction between the skin and the stiffener. The stress eigenfactors are similar to stress intensity factors in fracture mechanics, the latter being associated with square root singularities. Figure 6 shows the skin-stiffener interface peeling and shearing stress eigenfactors as a function of the applied pressure. The SEF has been normalized by the peeling stress eigenfactor for a 6.9-kPa linear analysis, hence, the notation $\bar{K}$. The influence of nonlinear effects is clearly illustrated in the figure. For a linear analysis, the SEF would simply be linearly proportional to the applied pressure. However, it is clear that the inclusion of geometric nonlinearities results in a different behavior.

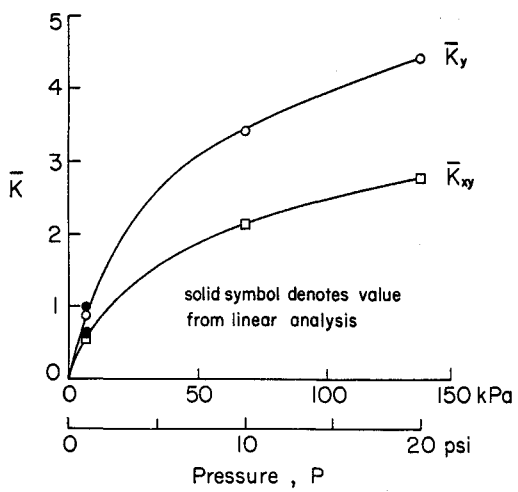

Fig. 6 Peeling and shearing stress eigenfactors as a function of applied pressure.

Specifically, the SEF increases slower than the applied pressure. This is consistent with the findings of Figs. 5, and both Figs. 5 and 6 point to the need for considering geometric nonlinearities in the study of skin-stiffener interaction. More important, it appears that, when conducting a failure analysis of such structures, it should be recognized that doubling the applied pressure does not result in a doubling of interface stresses, and to assume so would be erroneous. The stress eigenfactors also indicate that for the problem considered

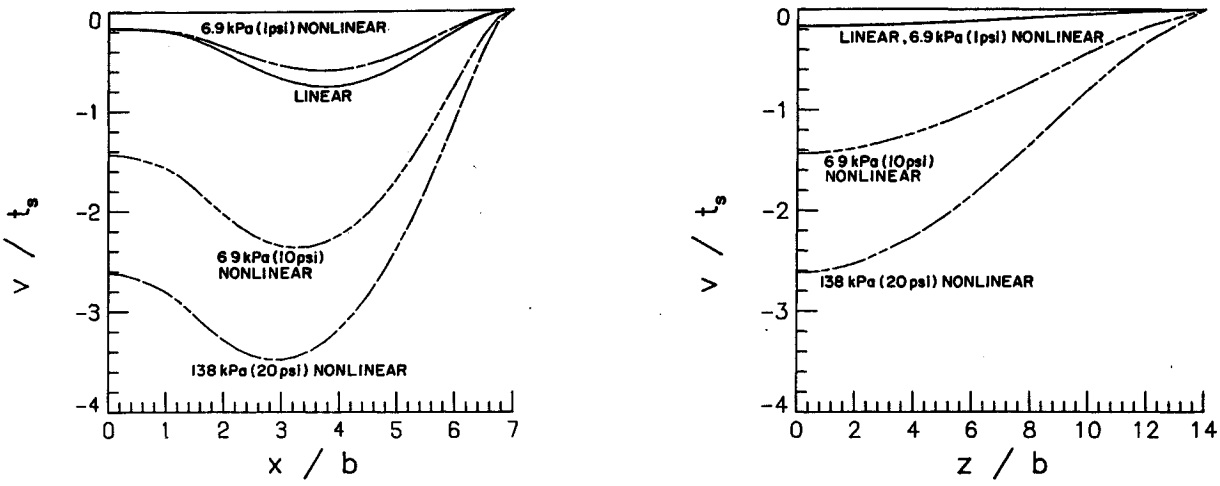

a) Transverse to stiffener along (x, 0, 0)

b) Collinear with stiffener along (0, 0, z)

Fig. 7 Out-of-plane deformation of skin-stiffener.

here, including the specific geometric and material parameters, the peel stress intensity factor is larger than the shear stress intensity factor, though both certainly contribute to failure of the skin-stiffener interface.

Finally, the influence of geometric nonlinearities on the plate out-of-plane deformations is considered in Figs. 7. Figures 7 consist of two portions, one depicting the out-of-plane deformation transverse to the stiffener along the symmetry line (x, 0, 0), and the other depicting the deformation under the web, collinear to the stiffener, along the symmetry line (0, 0, z). Both Figs. 7a and 7b illustrate four relations, one representing a linear analysis at 6.9-kPa pressure, and the other three corresponding to the nonlinear analyses at 6.9-, 69-, and 138-kPa applied pressure. The out-of-plane deformation v is normalized by the skin thickness t_s. The distance from the plate center (in the directions x or z) is normalized by the flange half-width b.

Evident in Fig. 7a is the fact that transverse to the stiffener, the skin under the stiffener, $x/b = 0$, deflects out-of-plane much less than the skin away from the stiffener, say at $x/b = 3$. This phenomenon is known as pillowing and it clearly is responsible for the skin tending to pull away from the stiffener. What is illustrated by the out-of-plane deflection profile of Figs. 7 is the fact that, at 6.9-kPa applied pressure, the maximum deflection of the skin occurs at $x/b = 3.9$ and the ratio of this maximum deflection to the deflection under the stiffener is 3.75. At 138 kPa, the maximum skin deflection moves toward the stiffener, to $x/b = 3$, and the ratio of the maximum deflection to the deflection under the stiffener is 1.3. Geometrically nonlinear effects clearly flatten the panel in the transverse direction and lessen the tendency of the skin to pull away from the stiffener. Figure 7b indicates that the panel also tends to flatten some in the stiffener direction. The flattening of the panel with increasing pressure is responsible for the redistribution of the stresses seen in Figs. 5b and 5d and the less-than-proportional increase in severity of the stress eigenfactors with increasing pressure, as seen in Fig. 6.

Conclusions

In the present paper, a previously developed approach for computing skin-stiffener interface stresses in the geometrically linear range was extended to include geometric nonlinearities. As in previous papers, particular attention was given to the flange termination region, a region where the stresses are high due to geometric and material discontinuities associated with this location. In the extension of the local elasticity solution to include geometrically nonlinear effects, the condition of small strains but moderate rotations was assumed. It was further assumed that the rotations were spatially uniform within the local region. This approach was applied to an actual stiffened composite plate structure. It was found that geometrically nonlinear effects influenced the calculation of interface stresses to a large degree. Thus, the use of geometrically linear analysis, rather than nonlinear analysis, can lead to considerable errors in the computing interface stresses. It should be noted that one specific problem was solved, namely, a pressure-loaded clamped plate. To solve other problems, e.g., a plate subjected to in-plane compressive loads, the procedure is identical. The specific problem being solved begins at the structural level analysis. The boundary conditions and applied loads for that problem dictate what is happening in the region of the plate that is referred to as the substructure region. The response in this region then determines the response in the local region. Although the stresses at the skin-stiffener interface do indeed depend on the conditions imposed on the original structural level problem, the mechanics that govern the interfaces stresses and the procedure for determining them are as outlined in this paper. Thus, what has been presented is a general procedure illustrated with results for a specific problem.

Acknowledgments

This study was supported by the NASA-Virginia Tech Composites Program under NASA Grant NAG-1-343. The authors would like to acknowledge, in particular, J. H. Starnes Jr. and M. P. Nemeth of NASA Langley Research Center for their useful contributions and support of this project.

References

[1]Knight, N. F., Jr., and Starnes, J. H., Jr., "Postbuckling Behavior of Selected Curved Stiffened Graphite-Epoxy Panels Loaded in Compression," *Proceedings of the 26th AIAA/ASME/ASCE/AHS Structures, Structural Dynamics, and Materials Conference*, AIAA, New York, April 1985.

[2]Hyer, M. W., and Cohen, D., "Calculation of Stresses and Forces Between the Skin and Stiffener in Composite Panels," *Proceedings of the 28th AIAA/ASME/ASCE/AHS Structures, Structural Dynamics, and Materials Conference*, AIAA, Washington, DC, April 1987.

[3]Hyer, M. W., and Cohen, D., "Calculation of Stresses and Forces Between the Skin and Stiffener in Composite Panels," *AIAA Journal*, Vol. 26, No. 7, 1988, pp. 852–858.

[4]Loup, D. C., Hyer, M. W., and Starnes, J. H., Jr., "Stiffener-Skin Interaction in Pressure Loaded Composite Panels," *Proceedings of the 27th AIAA/ASME/ASCE/AHS Structures, Structural Dynam-*

ics, and Materials Conference, AIAA, New York, May 1986.

[5]Whetsone, W. D., *EAL Engineering Analysis Language Reference Manual*, Engineering Information Systems, San Jose, CA, 1979.

[6]Lekhnitskii, S. G., *Theory of Elasticity of an Anisotropic Elastic Body*, Holden-Day, San Francisco, CA, 1963.

[7]Wang, S. S., and Choi, I., "Boundary Layer Effects in Composite Laminates; Part I—Free Edge Stresses," *Journal of Applied Mechanics*, Vol. 49, No. 3, 1982, pp. 540–548.

[8]Delale, F., "Stress Singularity in Bonded Anisotropic Materials," *International Journal of Solids and Structures*, Vol. 20, No. 1, 1984, pp. 31–40.

[9]Williams, J. H., Jr., "Stresses in Adhesive Between Dissimilar Adherents, *Journal of Adhesion*, Vol. 7, No. 2, 1975, pp. 97–107.

[10]Bogy, D. B., "Two Edge-Bonded Elastic Wedges of Different Materials and Wedge Angles Under Surface Traction, *Journal of Applied Mechanics*, Vol. 38, No. 2, 1971, pp. 377–386.

[11]Cohen, D., and Hyer, M. W., "Calculation of Skin-Stiffener Interface Stresses in Stiffened Composite Panels," Virginia Polytechnic Inst. and State Univ., Center for Composite Materials and Structures, Rept. CCMS-87-17, Blacksburg, VA, Dec. 1987.